Smart Structures and Systems, Vol. 11, No. 2 (2013) 217-240
DOI: http://dx.doi.org/10.12989/sss.2013.11.2.217

Damage detection in beam-type structures via PZT's dual piezoelectric responses

Khac-Duy Nguyen[1], Duc-Duy Ho[2] and Jeong-Tae Kim*[1]

[1]Department of Ocean Engineering, Pukyong National University, Busan, Korea
[2]Faculty of Civil Engineering, Ho Chi Minh City University of Technology, Vietnam

(Received November 9, 2011, Revised September 16, 2012, Accepted December 1, 2012)

Abstract. In this paper, practical methods to utilize PZT's dual piezoelectric effects (i.e., dynamic strain and electro-mechanical (E/M) impedance responses) for damage detection in beam-type structures are presented. In order to achieve the objective, the following approaches are implemented. Firstly, PZT material's dual piezoelectric characteristics on dynamic strain and E/M impedance are investigated. Secondly, global vibration-based and local impedance-based methods to detect the occurrence and the location of damage are presented. Finally, the vibration-based and impedance-based damage detection methods using the dual piezoelectric responses are evaluated from experiments on a lab-scaled beam for several damage scenarios. Damage detection results from using PZT sensor are compared with those obtained from using accelerometer and electric strain gauge.

Keywords: PZT's dynamic strain; E/M impedance; damage detection; structural health monitoring; beam structures

1. Introduction

Up to date, many damage detection methods have been developed on the basis of vibration and impedance characteristics (Adams *et al*. 1978, Stubbs and Kim 1996, Doebling *et al*. 1998, Kim *et al*. 2008, Gul and Catbas 2008, Koo 2008, Park *et al*. 2010, Kim *et al*. 2010). Vibration-based global damage detection methods utilize various vibration features such as time-history response, frequency response function, natural frequency, mode shape, modal strain energy, and modal flexibility (Pandey *et al*. 1991, Sohn and Farrar 2001, Sohn *et al*. 2003, Kim *et al*. 2003, Kim *et al*. 2006a, Catbas *et al*. 2006, Koo 2008, Nagayama *et al*. 2009). Once vibration signals are measured at distributed locations, those vibration features are extracted by using modal identification methods such as frequency domain decomposition (FDD) or stochastic subspace identification (SSI). Then, global damage detection is performed to identify damage occurrence in the entire structure and to estimate the location and the severity of damage.

For damage detection in local critical zones, both the direct and inverse effects of piezoelectric materials (e.g., PZT) are utilized to monitor the change in structural properties due to damage. Any changes in mechanical characteristics of host structures can be represented by the changes in

*Corresponding author, Professor, E-mail: idis@pknu.ac.kr

structural properties due to damage. Any changes in mechanical characteristics of host structures can be represented by the changes in electro-mechanical impedances measured by PZT sensors (Liang *et al*. 1996, Bhalla and Soh 2003, Park *et al*. 2003, Park *et al*. 2005, Giurgiutiu and Zagrai 2005). Once a PZT sensor is bonded to a local critical member, E/M impedance features such as real part, imaginary part, phase and magnitude are measured and utilized to alert damage occurrence in the local member by using statistical pattern recognition tools.

Both vibration-based and impedance-based methods have advantages in hybrid ways to efficiently detect damages in different geometrical scales. Currently, accelerometer and PZT sensor are employed to measure vibration and impedance responses, respectively. Considering the fact that dynamic strain can be passively measured and also E/M impedance can be actively generated from PZT sensors, the use of PZT sensors can be an alternative, cost-effective and convenient way for monitoring vibration and impedance responses. Recently, there have been a few research attempts to utilize the dual piezoelectric effects for damage detection in structures (Shanker *et al.* 2011). However, more efforts are still needed to investigate the feasibility of simple, practical, and reliable damage detection methods using PZT's dual piezoelectric responses.

This paper presents several practical methods to utilize PZT's dual piezoelectric responses for damage detection in beam-type structures. Firstly, PZT material's dual piezoelectric characteristics on dynamic strain and E/M impedance are investigated. Secondly, global vibration-based and local impedance-based methods for damage detection in beam-type structures are presented. The occurrence of damage is estimated by several indicators such as relative change in natural frequency, the correlation coefficient of power spectral densities of PZT's dynamic strains, and root mean square deviation (RMSD) of PZT's E/M impedance signatures. Also, the location of damage is predicted by a modal strain energy (MSE)-based damage index obtained from PZT's dynamic strain, and by a normalized RMSD index obtained from PZT's E/M impedance. Finally, the damage detection methods using the dual piezoelectric responses are evaluated by an experiment on a lab-scaled beam with several damage scenarios. The damage detection results from using PZT sensors are compared with those obtained from using accelerometers and electric strain gauges.

2. PZT's dynamic strain and E/M impedance responses

During the last decade, piezoelectric materials have been widely adopted for SHM in aerospace and civil engineering fields. The advantages of piezoelectric material are inexpensive, lightweight, robust, and multi-form ranging from thin patches to complex shapes (Giurgiutiu 2008). Piezoelectric materials are commonly used as passive sensors to measure dynamic strain or as active sensors to measure E/M impedance. The key characteristics of these dual piezoelectric responses are the utilization of the direct effect to sense structural deformation in addition to the inverse piezoelectric effect to actuate the structure.

2.1 PZT's dynamic strain responses

2.1.1 PZT's dynamic voltage versus PZT's dynamic strain

The principle of using piezoelectric materials as strain sensors is shown in Fig. 1. As the direct piezoelectric effect, an electric field is produced from a PZT patch due to a mechanical dynamic strain of the PZT. The constitutive relations for the PZT in 1-D mechanical interaction can be expressed as (Sirohi and Chopra 2000):

$$D_3 = \overline{e_{33}^{\sigma}} E_3 + d_{31}\sigma_1 \tag{1}$$

$$\varepsilon_1 = \frac{\sigma_1}{\overline{Y^E}} + d_{31}E_3 \tag{2}$$

where D_3 is the electric displacement in direction 3; $\overline{e_{33}^{\sigma}}$ is the dielectric constant of the PZT patch; E_3 is the applied external electric field in direction 3; d_{31} is the piezoelectric coupling constant; σ_1 is the stress in direction 1; ε_1 is the strain in direction 1; $\overline{Y^E}$ is the complex Young's modulus of the zero-electric field.

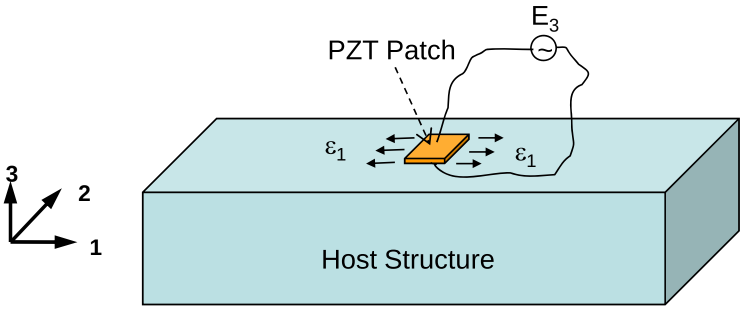

Fig. 1 1-D PZT-structure interaction in direct piezoelectric effect

If the PZT patch is desired to be used as a passive sensor only (without external electric filed across its terminals), the strain of the PZT patch can be expressed in terms of the voltage measured across its terminals as (Sirohi and Chopra 2000)

$$\varepsilon_1 = \left(\frac{\overline{e_{33}^{\sigma}}}{d_{31} t_p \overline{Y^E}} \right) V = k_p V \tag{3}$$

where V is the output voltage across the terminals of the PZT patch; t_p is the thickness of the PZT patch; k_p is the scale factor between strain and voltage which depends on the characteristics of the PZT patch. The output voltage V is easily measured by a voltage measurement system. For vibration-based damage detection, frequency response is usually extracted since it contains more important information of structural behaviors such as natural frequency and mode shape. Frequency response of the PZT's dynamic strain at location $x, \varepsilon_1(x,\omega)$, is obtained by the fast Fourier transform (FFT) of its time history response $\varepsilon_1(x,t)$

$$\varepsilon_1(x,\omega) = FFT[\varepsilon_1(x,t)] \tag{4}$$

By using Eq. (3), the dynamic strain is calculated from the dynamic voltage. However, in order to improve the accuracy of measurement, the output voltage of PZT sensor should be passed through some signal conditioning circuits (Sirohi and Chopra 2000). It should be noted that the derivation of Eq. (3) is based on the assumption that only 1-D strain contributes to the charge generated, the effect of other strain components is negligible, and that there is no loss of strain in the bond layer. In reality, however, a transverse component of strain exists and there are some losses in finite thickness bond layer (Sirohi and Chopra 2000, Bhalla *et al*. 2009). As a result, the value of strain as calculated by Eq. (3) is not the actual strain measured by a strain gauge. For this reason, some correction factors should be required to account for transverse strain and shear lag losses in the bond layer.

2.1.2 Calibration experiment for PZT's dynamic strain

In this study, an experiment was carried out to calibrate strain from output voltage of a PZT sensor. As shown in Fig. 2, the test beam is a lab-scaled 600×60×10 mm aluminum cantilever beam. A PZT sensor FT-20T-3.6A1 produced by APC International, Ltd, was installed at the fixed end location. Dynamic voltage from the PZT was measured by a data acquisition system which consists of a DAQ card, a terminal block and a PC with MATLAB software. For calibration, an electric strain gauge (ESG) TML FLA-5-11-1L was also placed at the fixed end location. The data acquisition system for the ESG consists of a bridge box TML SB120B, a universal recorder Kyowa EDX-100A and a PC with DCS-100A software. The impact force was applied at the location 180 mm distanced from the free end.

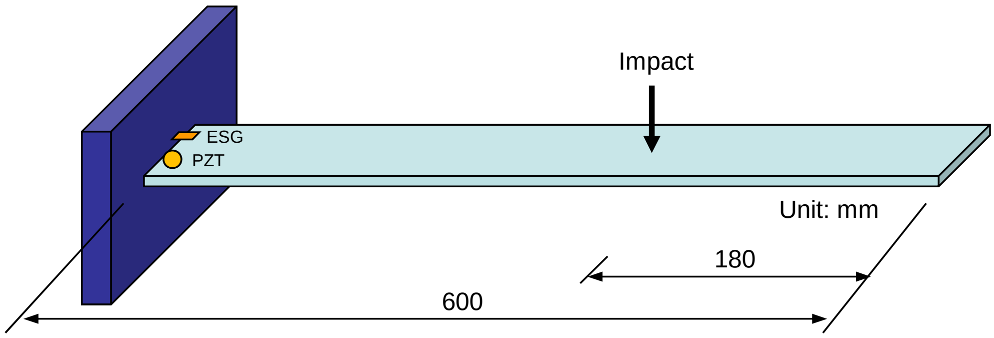

Fig. 2 Experiment setup for calibration of PZT's dynamic strain

Dynamic responses (i.e., PZT's voltage and ESG's strain) were measured at the same time with a sampling frequency of 1 kHz. Eight ensembles of PZT's voltage and ESG's strain due to different impact forces were recorded. Fig. 3 shows the time history responses measured by the PZT sensor and the ESG. The FFT frequency responses of PZT's voltage and ESG's strain are also shown in Fig. 4. In the time-domain responses (shown in Fig. 3), the maximum voltage measured by the PZT sensor was compared with the maximum strain measured by the ESG. Meanwhile, in the frequency-domain responses (shown in Fig. 4), the FFT spectrum area of the PZT's voltage was compared with that of the ESG's strain. As illustrated in Fig. 5, the PZT's voltage and the ESG's strain had a linear relationship in both time-domain and frequency-domain responses. Table 1 shows the scale factor between the ESG's strain and the PZT's voltage in time-domain and frequency-domain responses for eight tests. The scale factors between strain and voltage were almost consistent for the eight ensembles. Also, the scale factors obtained from time-domain responses were well agreed with those obtained from frequency-domain responses. Then, a mean scale factor of 17.5 was determined for calibrating strain response of the FT-20T-3.6A1 PZT sensor.

Table 1 Calibration of PZT's dynamic strain

Test No.	Time-domain			Frequency-domain		
	PZT	ESG	Scale factor	PZT	ESG	Scale factor
	V_{max} (V)	ε_{max} (μm/m)	k_p^t (μ/V)	*Voltage FFT Area (V.Hz)*	*Strain FFT Area* (μm/m.Hz)	k_p^f (μ/V)
1	4.98	85.2	17.1	4.56E+03	8.00E+04	17.5
2	4.36	76.3	17.5	4.33E+03	7.57E+04	17.5
3	4.23	73.3	17.3	4.20E+03	7.32E+04	17.4
4	4.73	82.0	17.3	4.74E+03	8.08E+04	17.1
5	3.36	60.3	17.9	3.43E+03	6.21E+04	18.1
6	3.75	67.1	17.9	3.74E+03	6.70E+04	17.9
7	4.61	80.4	17.4	4.64E+03	7.97E+04	17.2
8	5.0	88.3	17.7	5.13E+03	8.68E+04	16.9
Mean	-	-	17.5	-	-	17.5

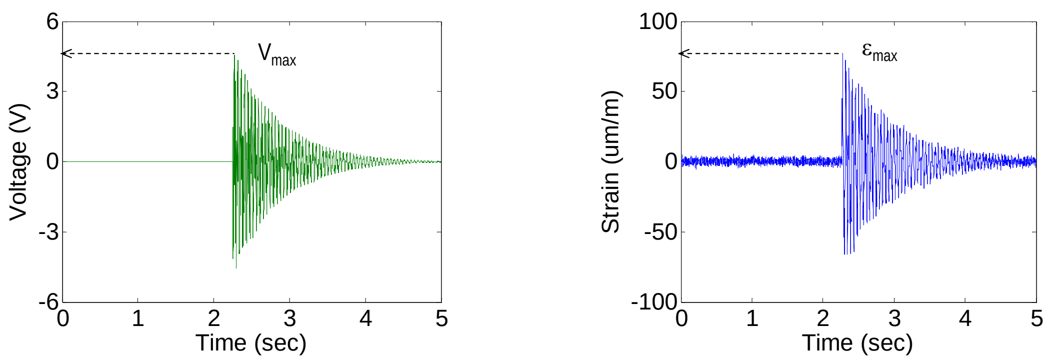

(a) PZT sensor: dynamic voltage (b) ESG: dynamic strain

Fig. 3 Time history responses of PZT sensor and ESG

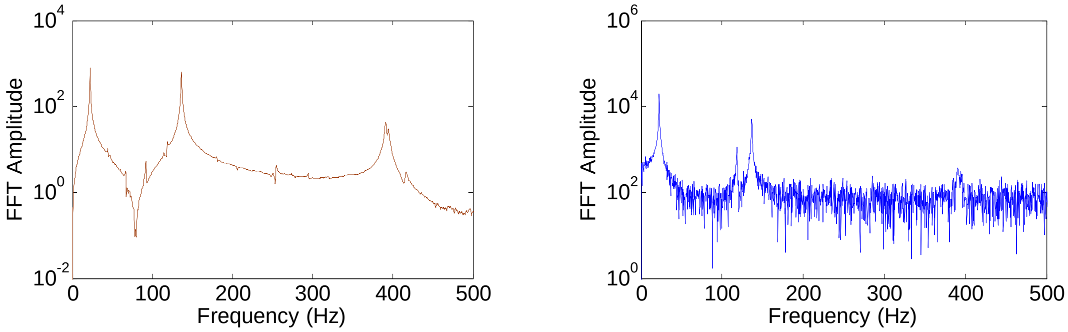

(a) PZT sensor: dynamic voltage (b) ESG: dynamic strain

Fig. 4 FFT frequency responses of PZT sensor and ESG

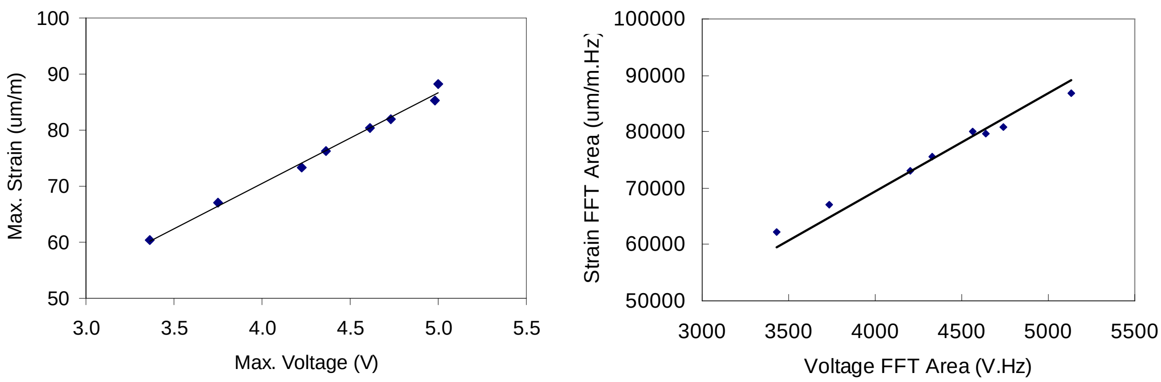

(a) PZT's max. voltage vs ESG's max. strain area (b) PZT's voltage FFT area vs ESG's strain FFT

Fig. 5 PZT sensor's dynamic voltage vs ESG's dynamic strain

2.2 PZT's impedance responses

Piezoelectric materials can also be used as active sensors for impedance measurement. The impedance responses measured by PZT patches are the coupling of mechanical and electrical features (Liang *et al*. 1996). Once a PZT patch is surface-bonded to a host structure, electrical effect of the PZT patch is partly controlled by mechanical effect of the host structure. As shown in Fig. 6, the interaction between the PZT patch and the host structure is conceptually explained as an idealized 1-D electro-mechanical relation. The host structure is described as the effects of mass, stiffness, damping, and boundary condition. The PZT patch is modeled as a short circuit powered by a harmonic voltage or current. The electrical admittance (the inverse of electro-mechanical impedance $Z(\omega)$) of the patch, $Y(\omega)$ (units Siemens or ohm^{-1}), is a combined function of the mechanical impedance of the host structure, $Z_s(\omega)$, and that of the piezoelectric patch, $Z_a(\omega)$, as follows

$$Y(\omega)= j\omega\frac{w_p l_p}{t_p}\left(\left(\overline{e_{33}^{\sigma}}-d_{31}^2\overline{Y_{11}^E}\right)+\frac{Z_a(\omega)}{Z_a(\omega)+Z_s(\omega)}d_{31}^2\overline{Y_{11}^E}\left(\frac{\tan kl_p}{kl_p}\right)\right) \tag{5}$$

where $\overline{Y_{11}^E}=(1+j\eta)Y_{11}^E$ is the complex Young's modulus of the PZT patch at zero-electric field; $\overline{e_{33}^{\sigma}}=(1-j\delta)e_{33}^{\sigma}$ is the dielectric constant of the PZT patch; d_{31} is the piezoelectric coupling constant in the direction-1 at zero stress; $k=\omega\sqrt{\rho/\overline{Y_{11}^E}}$ is the wave number that depends on mass density ρ and Young's modulus $\overline{Y_{11}^E}$ of the PZT patch; and w_p, l_p, and t_p are the width, length, and thickness of the PZT patch, respectively. The parameters η and δ are structural damping loss factor and dielectric loss factor of PZT patch, respectively.

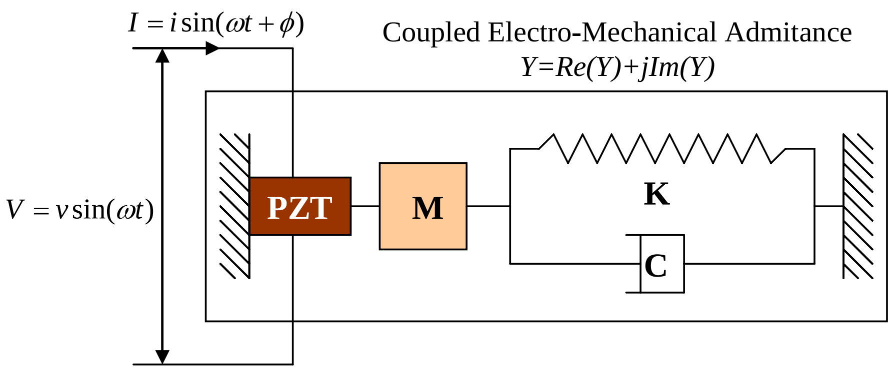

Fig. 6 1-D model electro-mechanical interaction between piezoelectric patch and host structure (Liang *et al.* 1996)

In Eq. (5), the first term is the capacitive admittance of the free PZT patch. The second term includes the mechanical impedance of both the PZT patch and the host structure. The mechanical impedance of the host structure $Z_s(\omega)$ is the ratio of PZT force, f_{PZT}, to structural velocity, $\dot{x}_{PZT}$, at PZT location, as follows

$$Z_s(\omega)=\frac{f_{PZT}}{\dot{x}_{PZT}}=\frac{F_{PZT}e^{i\omega t}}{\dot{x}_{PZT}} \tag{6}$$

If the structure is considered as a system of single degree of freedom, the mechanical impedance of the host structure can be expressed as

$$Z_s(\omega)=m\omega j+c-\frac{k}{\omega}j \tag{7}$$

Eq. (7) shows that the mechanical impedance of the host structure is a function of mass (m), stiffness (k) and damping (c). Therefore, any changes in dynamic characteristics of the structure could be represented by the change in E/M impedance.

3. Vibration and impedance-based damage detection methods

3.1 Design of damage detection scheme via dual piezoelectric responses

Hybrid SHM methods have been proposed by many researchers. The methods are based on the use of multiple physical quantities of a structure to assess its health status. Kim *et al.* (2006) proposed a hybrid algorithm utilizing acceleration and impedance features to detect different damage types in plate-girder bridges. Park *et al*. (2010) further examined the applicability of the combined use of acceleration and impedance signatures for damage monitoring of prestressed concrete girders. Also, Sim *et al*. (2011) accommodated both acceleration and strain measurements for SHM of truss structures.

As schematized in Fig. 7, on the basis of the previous studies, a hybrid SHM method utilizing PZT's dual piezoelectric responses such as dynamic strain and E/M impedance is implemented for beam-type structures. In the hybrid SHM scheme, the global vibration-based damage monitoring for an entire beam is performed in a parallel manner with the local impedance-based damage monitoring for beam elements. Firstly, vibration-based damage monitoring is performed in four steps: dynamic strain measurement for distributed locations, vibration feature extraction for the entire beam, global damage-occurrence alarming, and damage localization. Secondly, impedance-based damage monitoring is also performed in four steps: impedance measurement for the distributed beam elements, impedance feature extraction, local damage-occurrence alarming, and damage localization. Finally, the final decision is made by combining the results of the two approaches. The advantage of this method is that structural dynamic strain as passive response and E/M impedance of PZT-structure system as active response can be monitored by a single PZT sensor. Hence, the cost of sensor system can be greatly reduced. Note that, a PZT sensor itself is much cheaper than an accelerometer.

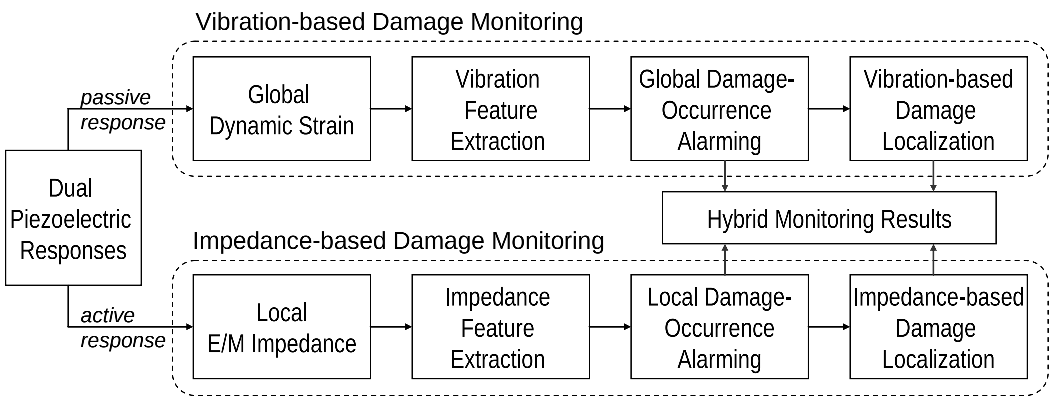

Fig. 7 Schematic of hybrid SHM via dual piezoelectric responses

3.2 Vibration-based damage detection methods

In this study, three vibration-based SHM methods are utilized for global damage detection purpose. The three methods are 1) damage alarming by relative change in natural frequency, 2) damage alarming by correlation coefficient of power spectral densities (Kim *et al*. 2010), and 3) damage localization by modal strain energy-based damage index (Kim *et al*. 2003). Below the three methods are modified for the use of dynamic strain responses.

3.2.1 Damage alarming by relative change in natural frequency

Natural frequency is one of vibration parameters of structural systems. It is easily determined by picking peaks in frequency domain of acquired time signals, or by using modal identification methods such as frequency domain decomposition (FDD) and stochastic subspace identification (SSI) (Brincker *et al*. 2001, Yi and Yun 2004). The relative change in natural frequency is commonly utilized for global damage alarming since it represents global property of an entire structure. The relative change in the i^{th} natural frequency before and after the occurrence of damage is defined as

$$\frac{\delta f_i}{f_i} = \frac{f_i^* - f_i}{f_i} \times 100\% \tag{8}$$

where f_i, f_i^* are the i^{th} natural frequency before and after damage, respectively.

3.2.2 Damage alarming by correlation coefficient of power spectral densities

The power spectral density (PSD) of a vibration signal may contain less noise than the ordinary fast Fourier transform (FFT) result since it is computed from the average of FFT results. The PSD of a dynamic strain $S_\varepsilon(x,\omega)$ at location *x* can be calculated as (Bendat and Piersol 1993)

$$S_\varepsilon(x,\omega) = \frac{1}{n_d T}\sum_{i=1}^{n_d} \left|\varepsilon_i(x,\omega)\right|^2 \tag{9}$$

where $\varepsilon_i(x,\omega)$ is dynamic responses transformed into frequency domain (FFT of a time history of dynamic strain $\varepsilon_i(x,t)$); n_d is the number of divided segments in the time history; and T is the data length of a divided segment.

For damage-occurrence alarming, the correlation coefficient of PSDs obtained before and after a damaging incident is calculated by (Kim *et al*. 2010)

$$\rho_\varepsilon = \frac{E\left[S_\varepsilon(x,\omega)S_\varepsilon^*(x,\omega)\right] - E\left[S_\varepsilon(x,\omega)\right]E\left[S_\varepsilon^*(x,\omega)\right]}{\sigma[S_\varepsilon]\sigma[S_\varepsilon^*]} \tag{10}$$

where $E[\bullet]$ is the expectation operator; and $\sigma[S_\varepsilon]$ is the standard deviation of the PSD, respectively. Note that the asterisk (*) denotes the damaged state. A control chart analysis is used to discriminate damage from the correlation coefficient values. The lower control limit (*LCL*) is determined as $LCL = \mu_\rho - 3\sigma_\rho$, in which μ_ρ and σ_ρ are the mean and the standard deviation of the correlation coefficients obtained at the undamaged state, respectively.

3.2.3 Damage localization by modal strain energy-based damage index

Modal strain energy (MSE) is one of damage sensitive features which can be obtained by measuring mode shape or mode shape curvature. Stubbs and Kim (1996), Kim *et al.* (2003) proposed an MSE-based damage detection method using the fractional change in MSE. For a beam structure, damage in the j^{th} member is defined as the relative change between undamaged flexural stiffness, k_j, and damaged one, k_j^*, of the same element. For M available vibration modes, the MSE-based damage index for j^{th} location, β_j, is given by

$$\beta_j = k_j \Big/ k_j^* = \sum_{i=1}^{M} \gamma_{ji}^* \Big/ \sum_{i=1}^{M} \left(\gamma_i g_i + \gamma_{ji}\right) \tag{11}$$

where g_i $(= \delta\omega_i^2 / \omega_i^2)$ represents the fractional changes in the i^{th} natural frequencies; the terms γ_i and γ_{ji} are the i^{th} modal stiffness and the contribution of the j^{th} element to the i^{th} modal stiffness, respectively.

When acceleration signals are measured, γ_i and γ_{ji} are calculated from displacement mode shapes extracted from experimental modal analysis as (Kim *et al*. 2003)

$$\gamma_{ji} = \Phi_i^T \mathbf{C}_{j0} \Phi_i \text{, and } \gamma_i = \sum_{j=1}^{NE} \Phi_i^T \mathbf{C}_{j0} \Phi_i \tag{12a}$$

where NE is the number of elements, Φ_i is the i^{th} displacement mode shape, and $\mathbf{C}_{j0}$ is the geometric quantities of the j^{th} element contributed to system stiffness matrix that can be computed numerically.

When dynamic strains are measured, the corresponding γ_i and γ_{ji} are calculated from extracted strain mode shapes on the basis of Euler-Bernoulli beam theory

$$\gamma_{ji} = \int_j c_{j0} \left[\Psi_i(x)\right]^2 dx \text{, and } \gamma_i = \sum_{j=1}^{NE} \int_j c_{j0} \left[\Psi_i(x)\right]^2 dx \tag{12b}$$

where $\Psi_i(x)$ is the i^{th} strain mode shape and c_{j0} is the j^{th} element stiffness that can be computed by knowing the geometric properties of the element.

Treating the MSE-based damage indices as random variables, the normalized damage indices are defined according to the standard rule as

$$Z_j = \left(\beta_j - \mu_\beta\right) / \sigma_\beta \tag{13}$$

where μ_β and σ_β are the mean and the standard deviation of the collection of β_j values, respectively. Then, the damage is localized from statistical hypothesis tests. The null hypothesis (i.e., H_o) is taken to be the structure undamaged at j^{th} element and the alternate hypothesis (i.e., H_1) is taken to be the structure damages at j^{th} element. In assigning damage to a particular location, the following decision rule is utilized: first, choose H_1 if $Z_j \geq Z_o$; or choose H_o if $Z_j < Z_o$, where Z_o is statistical confidence level of the localization test. As a result, the damage is assigned to the j^{th} location if Z_j exceeds the confidence level.

3.3 Impedance-based damage detection methods

Two impedance-based SHM methods are utilized for local damage detection purpose. The two methods are 1) damage alarming by root mean square deviation (RMSD) of impedance signatures (Sun *et al*. 1995), and 2) damage localization by normalized RMSD index. The normalized RMSD index is newly proposed to detect damage location via statistical pattern recognition of impedance signatures.

3.3.1 Damage alarming by RMSD of impedance signatures

For damage-occurrence detection, RMSD of impedance signatures is selected to quantify damage-induced change in impedance signatures. The RMSD is calculated from the impedance signatures measured before and after damage as (Sun *et al*. 1995)

$$RMSD(Z, Z^*) = \sqrt{\sum_{i=1}^{N} \left[Z^*(\omega_i) - Z(\omega_i)\right]^2 \Big/ \sum_{i=1}^{N} \left[Z(\omega_i)\right]^2} \tag{14}$$

where $Z(\omega_i)$ and $Z^*(\omega_i)$ are the impedance measured before and after damage for the i^{th} frequency, respectively; and N denotes the number of frequency points in the sweep. The RMSD equals to 0 if no damage. Otherwise, the RMSD is larger than 0.

Due to experimental and environmental uncertainties, however, the RMSD may be larger than 0 although no damage occurs. To deal with the uncertain conditions, the upper control limit is determined as a damage alarming threshold using the RMSD data at the undamaged state. The upper control limit (*UCL*) is calculated as: $UCL = \mu[RMSD] + 3\sigma[RMSD]$, in which $\mu[RMSD]$ and $\sigma[RMSD]$ are respectively the mean and the standard deviation of the RMSD data set obtained from a PZT at the undamaged state. The occurrence of damage is indicated when the RMSD values are larger than the *UCL*. Otherwise, there is no indication of damage occurrence.

3.3.2 Damage localization by normalized RMSD index

As the next stage, damage localization should be performed once damage occurrence is alerted. Generally, an impedance response of a PZT sensor located nearby a certain damage is changed more sensitively than other impedance responses measured far from the damage (Park *et al*. 2000, Zagrai and Giurgiutiu 2001). In the previous study by Park *et al*. (2006), damage in the flange of an I-shaped steel truss member was detected at the PZT's location where the RMSD level of that PZT exceeded 10%. However, the utilization of a constant value (e.g., 10%) as a threshold may lead to false localization since the RMSD level can reach to the threshold due to the increment of damage severity as well. In order to overcome this limitation, a statistical pattern recognition concept is utilized to detect the location of damage by considering the RMSD indices ($RMSD_j$; j=1, N) as random variables with a normal distribution. As similar to Eq. (13), $RMSD_j$ is normalized by the standard rule as follows

$$Z_j^{RMSD} = \frac{RMSD_j - \mu[RMSD_j]}{\sigma[RMSD_j]} \tag{15}$$

where $\mu[RMSD_j]$ and $\sigma[RMSD_j]$ are the mean and standard deviation of the collection of $RMSD_j$ values, respectively. As similar to the previous description, the damage is localized from statistical hypothesis tests. Firstly, Z_o^{RMSD} is defined as a statistical criterion depending upon the confidence level of the localization test. Next, the damage is located at position of the j^{th} PZT if $Z_j^{RMSD} > Z_o^{RMSD}$; otherwise, damage is located at elsewhere. On the other words, the damage is assigned to the j^{th} location if Z_j^{RMSD} exceeds the confidence level.

4. Experimental verification of damage detection via dual piezoelectric responses

4.1 Experimental setup and damage scenarios

The feasibility of utilizing PZT's dynamic strain and E/M impedance responses for the vibration and impedance-based damage detection is examined on a lab-scaled beam. Dynamic tests were performed on a 600×60×10-mm aluminum cantilever beam as shown in Fig. 8. Five PZT sensors were attached along the beam with a constant interval of 150 mm. The impact force was applied at the location 180 mm distanced from the free end. For comparison, five accelerometers and five ESGs were also installed at the same locations parallel with the PZT sensors. Three types of vibration signals were measured as acceleration from accelerometers, dynamic strain from PZT sensors, and dynamic strain from ESGs. Also, E/M impedance responses were measured from the same PZT sensors which were used for dynamic strain measurement.

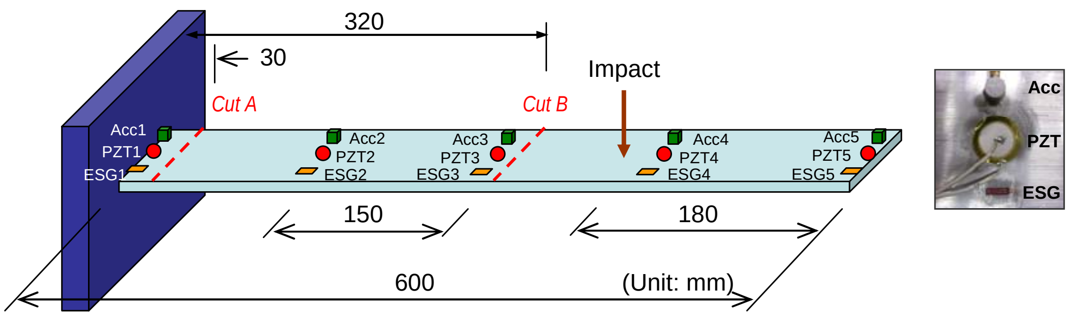

Fig. 8 Experiment setup for lab-scale beam

For dynamic strain measurement from PZT sensor, PZT sensors FT-20T-3.6A1 were used. The data acquisition system for PZT's dynamic strain consists of a DAQ card, a terminal block and a PC with MATLAB software. For acceleration measurement, accelerometers Dytran 3101BG with nominal sensitivities of 100 mV/g were used. The acceleration acquisition system consists of a 16-channel PCB signal conditional, a DAQ card, a terminal block and a PC with MATLAB software. For dynamic strain measurement from ESG, strain gauges TML FLA-5-11-1L were used. The data acquisition system consists of 5 bridge boxes TML SB120B, a universal recorder Kyowa EDX-100A and a PC with DCS-100A software. For impedance measurement from the PZT sensors, the data acquisition system consists of an impedance analyzer HIOKI 3532 and a PC with LabVIEW software.

The vibration signals (i.e., acceleration and dynamic strain) were recorded for 5 seconds with a sampling frequency of 1 kHz. The impedance signatures between 35 kHz and 85 kHz were measured from the PZT sensors with 500 intervals. Four damage cases were inflicted on the test beam as given in Table 2 and also depicted in Fig. 8. To simulate the damage, a cut was sawed on the beam at a location of 30 mm (i.e., cut A: x/L = 0.05) and another location of 320 mm (i.e., cut B: x/L = 0.53) from the fixed end. Also, two levels of damage-size were introduced with ratios of crack depth (a) to beam thickness (t) as 0.2 and 0.5. For each case, eight ensembles of vibration and impedance signatures were recorded. During the test, room temperature was kept close to constant as 23~24^{o}C by air conditioners.

Table 2 Damage scenarios on test beam

Case	Damage scenario	
Damage 1	Cut A (x/L=0.05; a/t = 0.2)	
Damage 2	Cut A (x/L=0.05; a/t = 0.5)	
Damage 3	Cut A (x/L=0.05; a/t = 0.5)	Cut B (x/L=0.53; a/t = 0.2)
Damage 4	Cut A (x/L=0.05; a/t = 0.5)	Cut B (x/L=0.53; a/t = 0.5)

4.2 Vibration-based damage monitoring

As described in Fig. 7, the vibration-based damage monitoring is performed by four steps as acquiring dynamic strain, extracting vibration feature, alarming damage occurrence and localizing damage. Fig. 9 shows the time history responses at sensor location 3 for three different sensor types. Frequency domain decomposition (FDD) method (Brincker *et al*. 2001) was employed to extract natural frequencies and mode shapes of the beam. Figs. 10 and 11 show frequency responses and mode shape curvatures obtained for the first three bending modes, respectively. It was observed that the responses of the three sensor types showed good agreement each other. It is also noted that the frequency response from the ESG contained very high noise in comparison with those from the accelerometer and the PZT sensor.

4.2.1 Damage alarming by relative change in natural frequency

The relative change in natural frequency was utilized to alert the occurrence of damage in the beam. The natural frequencies measured by the three sensor types (i.e., accelerometer, PZT sensor, and ESG) are given in Table 3. It was observed that the natural frequencies measured by PZT sensor were well matched with those measured by accelerometer and ESG. Natural frequencies were decreased as the severity of damage increased. For Damage 4 which was the most severe case, the natural frequencies reduced by 5.5%, 5.7%, and 1.5% for mode 1, mode 2, and mode 3, respectively. As summary, the occurrences of all damage scenarios were successfully alerted by the relative change in natural frequency.

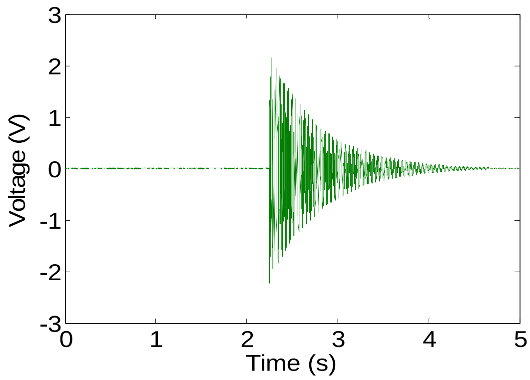

(a) PZT Sensor

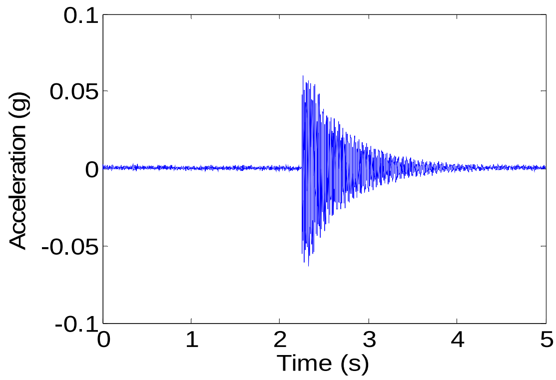

(b) Accelerometer

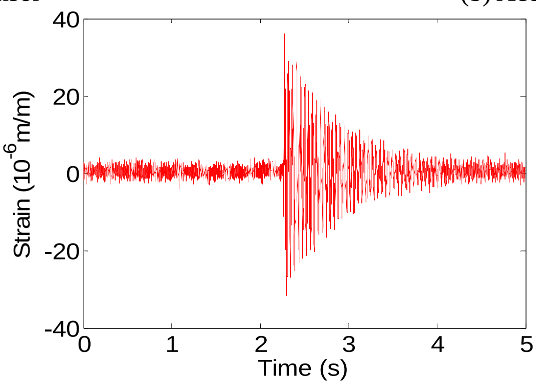

(c) ESG

Fig. 9 Time history responses of sensors at location 3

4.2.2 Damage alarming by correlation coefficient of power spectral densities

The correlation coefficient of PSDs was also utilized to alert the occurrence of damage in the test beam. For the undamaged and four damage states, as shown in Fig. 12, PSDs were computed from the vibration responses measured by the three sensor types at sensor location 3. It was observed that the PSDs changed due to the damages. As shown in Fig. 13, the correlation coefficients of PSDs were calculated by Eq. (10) in order to quantify the changes in the vibration responses. For the undamaged case, eight ensembles of PSDs were utilized to determine a lower control limit (*LCL*) for damage alarming. As shown in Fig. 13, all damage cases were successfully alerted by the three sensor types.

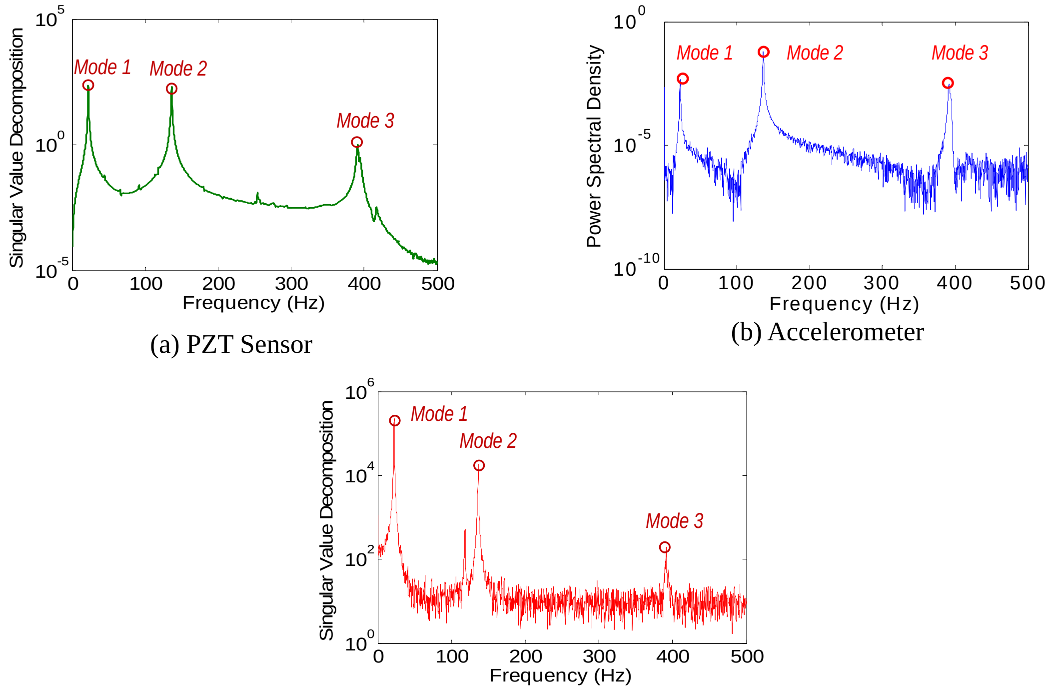

(a) PZT Sensor

(b) Accelerometer

(c) ESG

Fig. 10 Frequency responses of sensors at location 3

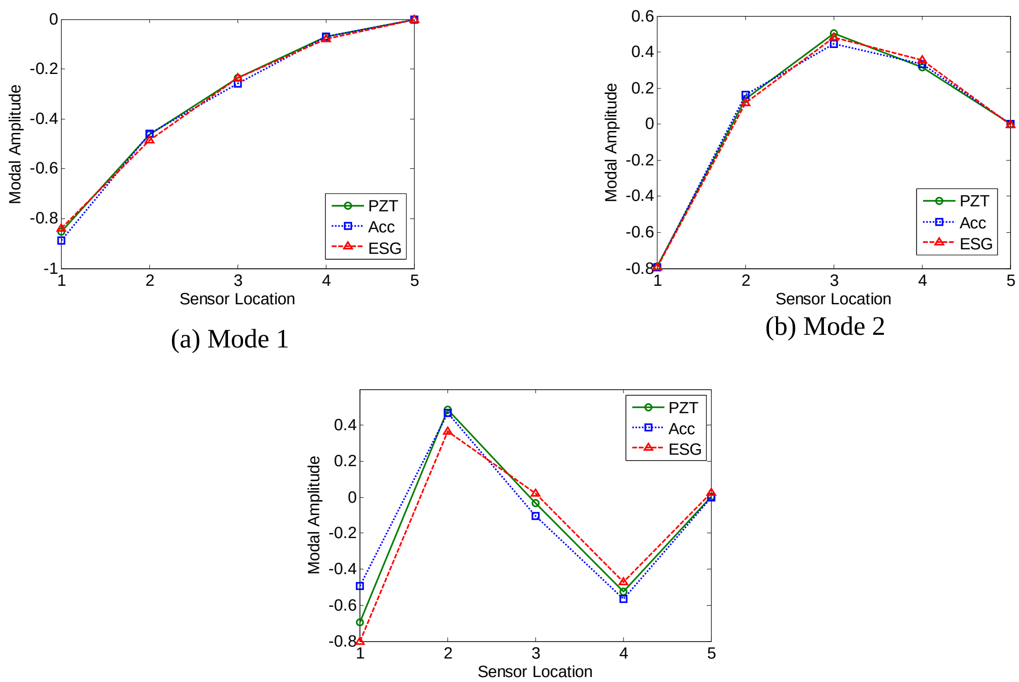

(a) Mode 1

(b) Mode 2

(c) Mode 3

Fig. 11 Mode shape curvatures of test beam

Table 3 Natural frequency (Hz) of test beam measured by three sensor types

Case	Acceleration			PZT sensor			Electrical strain gauge		
	Mode 1	Mode 2	Mode 3	Mode 1	Mode 2	Mode 3	Mode 1	Mode 2	Mode 3
Undamage	22.22	136.38	391.33	22.22	136.38	391.11	22.22	136.29	391.21
Damage 1	21.97	135.5	390.63	21.97	135.5	390.54	21.97	135.5	390.72
Damage 2	21.0	132.08	386.78	21.0	132.08	386.78	21.0	132.08	386.84
Damage 3	21.0	131.59	386.63	21.0	131.59	386.63	21.0	131.59	386.59
Damage 4	21.0	128.66	385.44	21.0	128.66	385.44	21.0	128.66	385.41

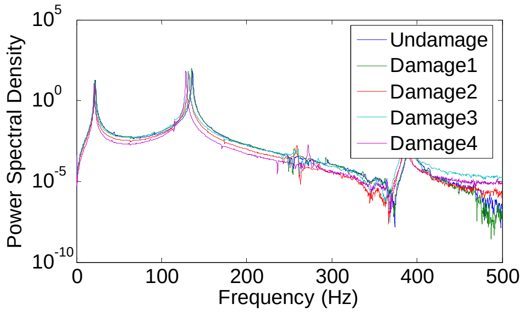

(a) PZT Sensor

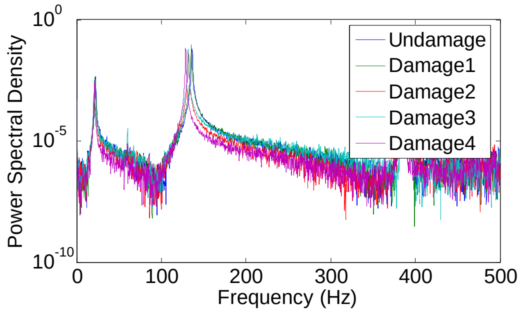

(b) Accelerometer

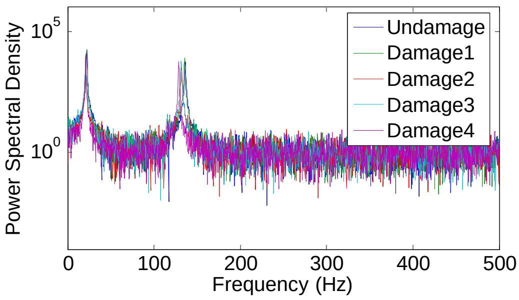

Fig. 12 Power spectral densities of sensors at location 3

4.2.3 Damage localization by modal strain energy-based damage index

After successful damage-occurrence alarming, the MSE-based damage monitoring method described previously was employed to estimate the location of damage in the beam. The damage localization indices were calculated by Eqs. (11) and (13) for the fractional change in MSE between the undamaged and the four damage cases. Here, the criterion value was determined as the unity (1) which is equivalent to the confidence level of 84%. Fig.14 shows MSE-based damage localization results for all damage cases by using PZT's dynamic strain. Damage localization for the damage cases with single damage location (i.e., Damage 1 and Damage 2) was successful.

Meanwhile, damage localization for the damage cases with two damage locations (i.e., Damage 3 and Damage 4) was partially successful. For Damage 3, the MSE-based method was able to locate only the significant damage at the fixed end, but was unable to locate the small damage in the middle of the beam. For Damage 4 with two significant damages, all two damage locations were accurately detected.

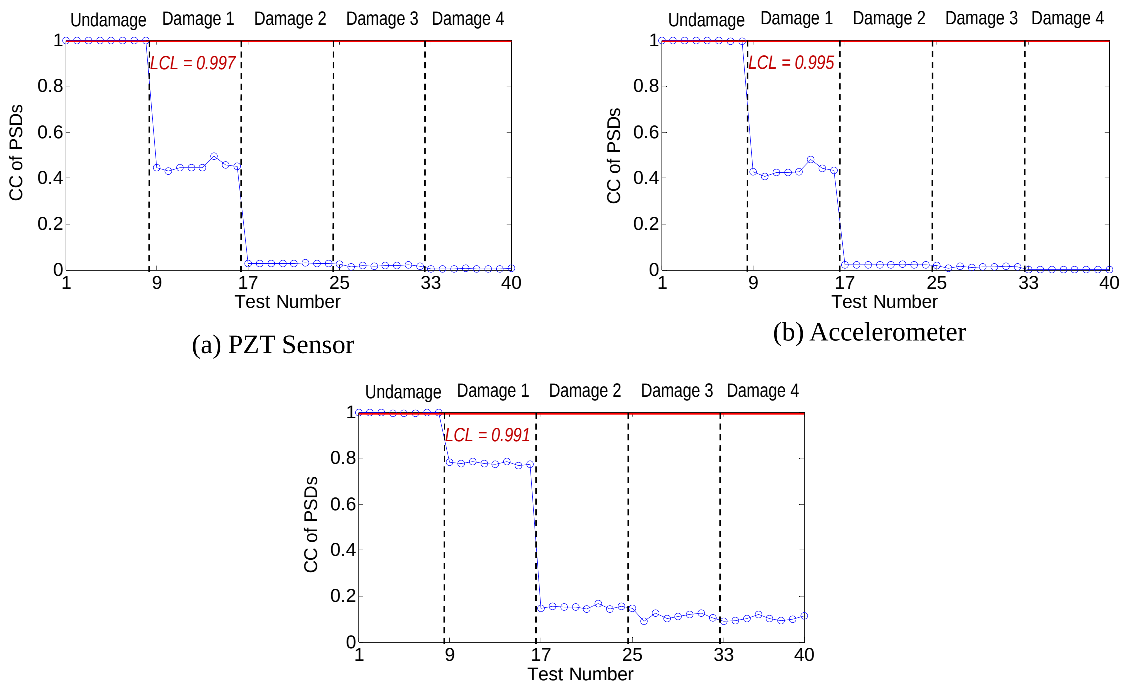

(a) PZT Sensor

(b) Accelerometer

(c) ESG

Fig. 13 Correlation coefficient of PSDs

For comparison, damage localization tasks were performed by using the accelerometers and the ESGs as shown in Figs. 15 and 16. As similar to the results of the PZT's dynamic strain, most of the acceleration's and ESG's predictions were accurate, except the unpredictable small sawed cut in the middle of the beam in Damage 3. It was also found that the confidence levels of damage localization from the PZT sensor were high and equivalent to those from the accelerometer for all damage cases. Meanwhile, the confidence level from the ESG for the sawed cut at the middle of the beam was rather smaller than those from the other sensor types.

4.3 Impedance-based damage monitoring

The utilization of E/M impedance measured from PZT sensors is an additional approach for alarming damage-occurrence and localizing damage in the beam. As described in Fig.7, the impedance-based damage monitoring is also performed by four steps as acquiring E/M impedance, extracting impedance feature, alarming damage occurrence and localizing damage. Fig. 17 shows real parts of impedance signatures measured from PZT1. As shown in Fig. 17(a), many peaks indicating resonant responses of the beam were observed in the frequency range 35 kHz – 85 kHz. By trial and error, impedance signatures in the narrower frequency range 45 kHz – 55 kHz (as shown in Fig. 17(b)) were found more sensitive to the damages than those in other ranges.

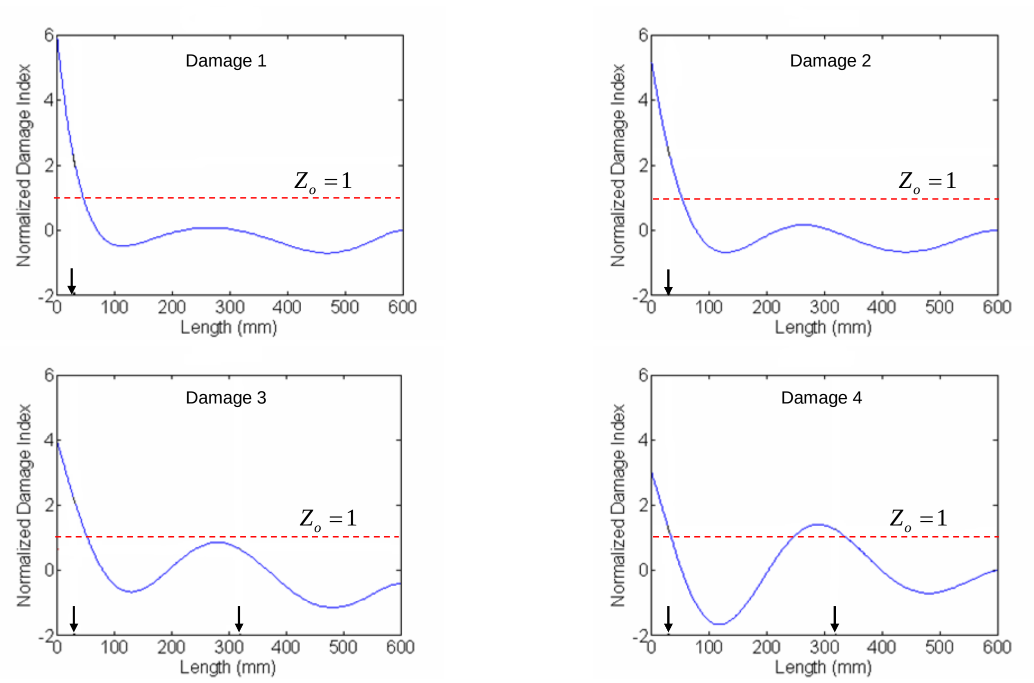

Fig. 14 MSE-based damage localization results using PZT's dynamic strain
(↓:: inflicted damage)

4.3.1 Damage alarming by RMSD of impedance signatures

The change in E/M impedance signatures was quantified to alert damage occurrence. As shown in Fig. 17(b), the real impedance signatures measured from PZT1 were shifted to the left side as the damage severity increased. The RMSD indices of impedance signatures calculated by Eq. (14) are shown in Fig. 18. Eight ensembles of the RMSD at undamaged state were used to determine the upper control limit (*UCL*) for damage alarming. As shown in Fig. 18, the occurrences of all four damage cases were successfully alerted.

4.3.2 Damage localization by normalized RMSD index

The location of damage was estimated using RMSD of impedance of all 5 PZT sensors on the beam. The normalized RMSD indices were calculated by Eq. (15) for damage localization. Here the RMSD criterion was also decided as the unity (equivalent to the confidence level of 84%). Fig. 19 shows the damage localization results for all damage cases. For the damage cases with single damage location, the use of normalized RMSD indices was successful to detect the location of the small damage in Damage 1, but it failed to localize the significant damage in Damage 2.

Meanwhile, damage localization for the damage cases with multiple damage locations was partially successful. It was failed to detect the significant damages at fixed end in Damage 3 and at middle of the beam in Damage 4.

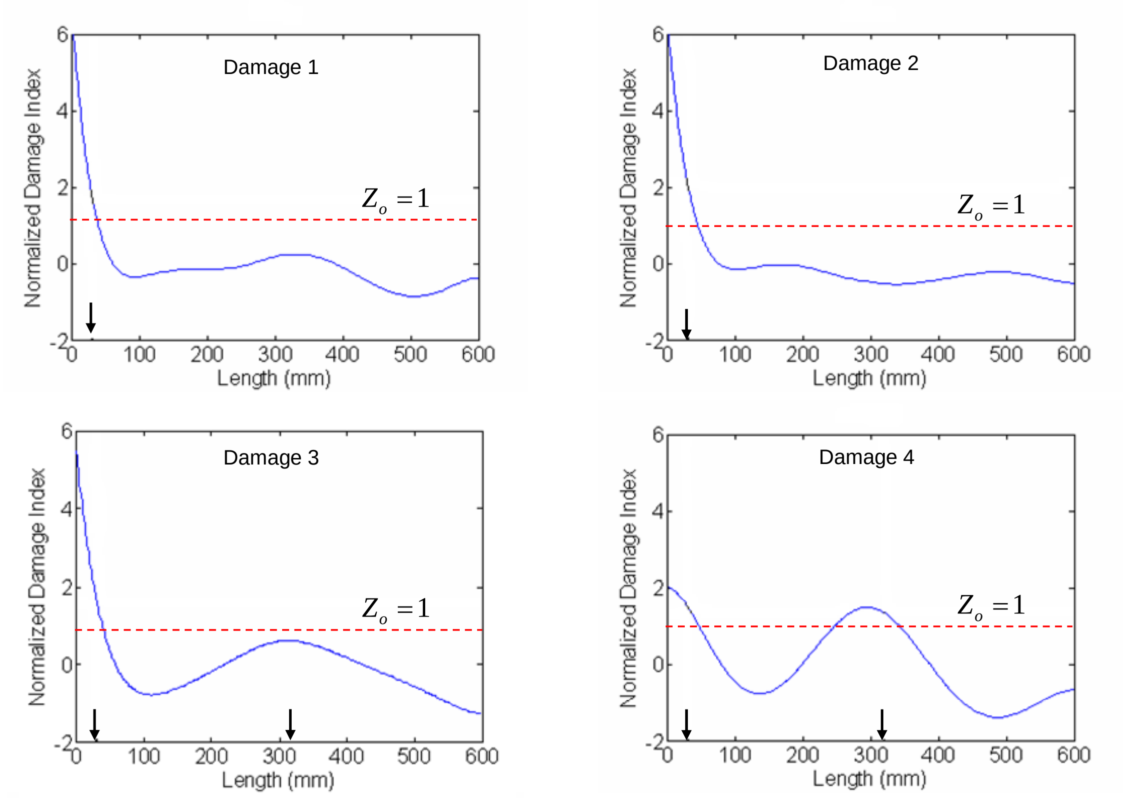

Fig. 15 MSE-based damage localization results using acceleration
(↓: inflicted damage)

5. Hybrid vibration-impedance monitoring results

As shown in Fig. 14 and Fig. 19, the vibration-based or the impedance-based SHM methods using PZT sensors were not individually successful to detect all the damages. It is observed from Fig. 14 that vibration-based damage localization method (e.g., MSE-index) was more feasible for the significant sawed cut (e.g., a/t = 0.5) than for small sawed cut (e.g., a/t = 0.2). Meanwhile, the impedance-based damage localization results (e.g., normalized RMSD) for small sawed cut were more accurate than those for significant sawed cut, as shown in Fig. 19. Hence, the combination of those methods (i.e., hybrid SHM) could give better results on the damage detection. Table 4 gives the summary of damage detection results by the vibration-based SHM, the impedance-based SHM and the hybrid SHM using the PZT sensors. As shown in the table, the occurrences of all damage cases were successfully alarmed by both the vibration-based SHM and the impedance-based SHM.

However, the locations of some damages were not successfully detected by using only dynamic strain or E/M impedance responses. By adopting the hybrid SHM concept as combining their results, the locations of the damages were better estimated as shown in the seventh column of Table 4.

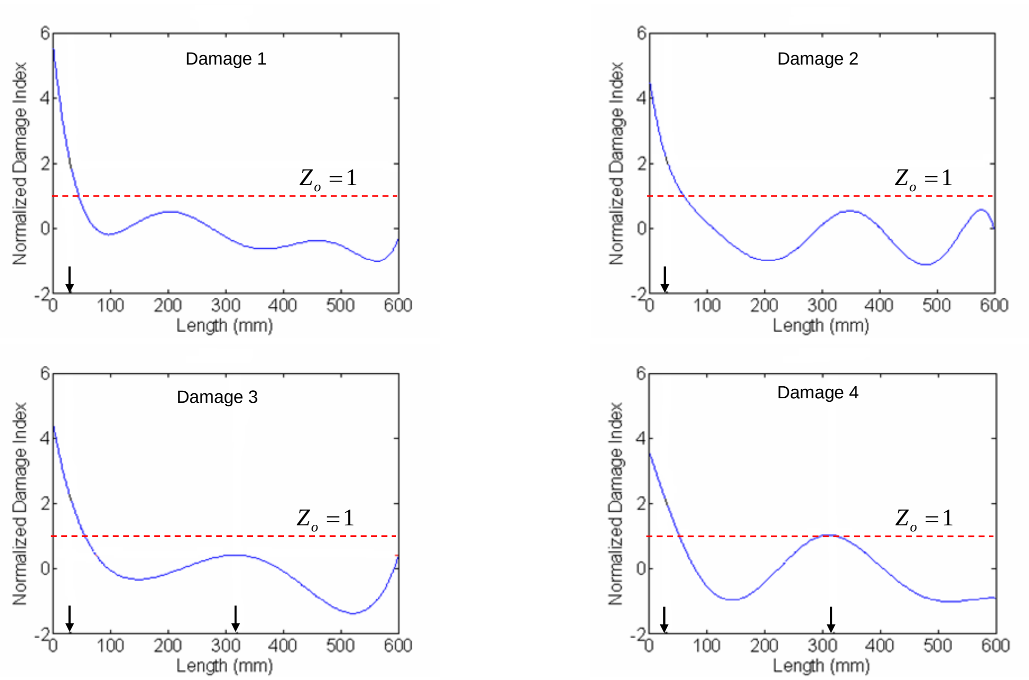

Fig. 16 MSE-based damage localization results using ESG's dynamic strain
(↓: inflicted damage)

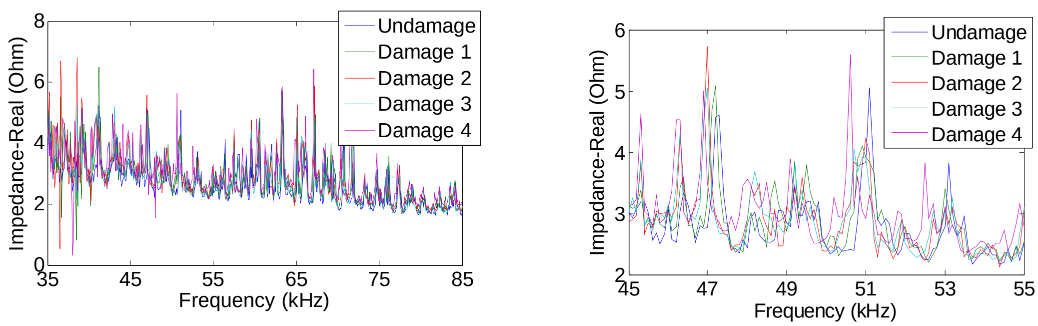

(a) Frequency Range: 35~85 kHz (b) Frequency Range: 45~55 kHz

Fig. 17 Real impedance signatures of PZT1 for four damage cases

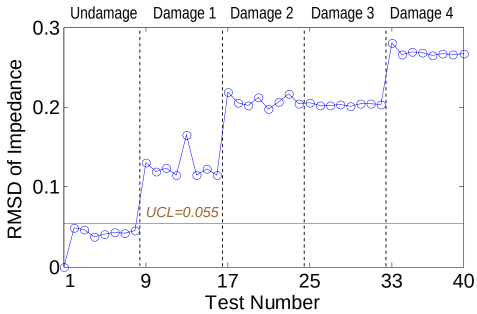

Fig. 18 RMSD of impedance signatures of PZT1 for four damage cases

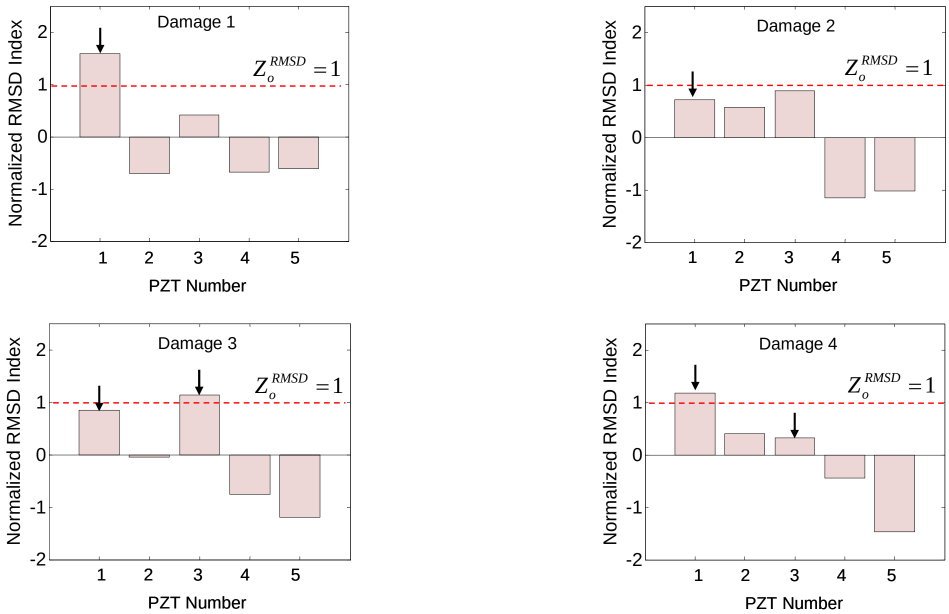

Fig. 19 Damage localization using normalized RMSD of impedance (↓: inflicted damage)

6. Conclusions

In this paper, practical methods to utilize PZT's dual piezoelectric effects (i.e., dynamic strain and E/M impedance responses) for damage detection in beam-type structures were presented. Firstly, PZT material's dual piezoelectric characteristics on dynamic strain and E/M impedance were investigated. Secondly, global vibration-based and local impedance-based methods for damage detection in beam-type structures were presented. The vibration-based methods included relative change in natural frequency and the correlation coefficient of PSDs for damage alarming, and the MSE-based damage index for damage localization. The impedance-based methods included RMSD of impedance signatures for damage alarming, and the normalized RMSD index for damage localization. Finally, the damage detection methods using the dual piezoelectric responses were evaluated by an experiment on a lab-scaled beam with several damage scenarios.

From the experimental results, the following conclusions have been made. PZT sensors showed good performance on dynamic strain measurement compared with electric strain gauges. The occurrences of all damage cases in the lab-scaled beam were successfully alerted by using PZT's dynamic strain or E/M impedance. However, the vibration-based method using PZT's passive responses or the impedance-based method using PZT's active responses showed limitations on damage localization. It was found that the vibration-based localization method was more feasible to detect significant damages, while the impedance-based localization method performed better for small damages. As the combination of the two methods, the hybrid SHM method showed better capability on damage localization. The use of PZT's dual piezoelectric responses is promising for hybrid SHM applications since PZT sensors are utilized as global vibration sensors and local impedance sensors.

Table 4 Summary of damage detection results

Case	Vibration-based SHM			Imp.-based SHM		Hybrid SHM
	Freq. Shift	CC of PSD	MSE Index	RMSD	Norm. RMSD	
Damage 1	☐	☐	○	☐	○	○
Damage 2	☐	☐	○	☐	✕	○
Damage 3	☐	☐	⊙	☐	⊙	●
Damage 4	☐	☐	●	☐	⊙	●

☐: Damage occurrence is successfully alarmed
○: Single damage is successfully localized
✕: Single damage is undetectable
●: All two damages are successfully localized
⊙: One damage is successfully localized, one other is undetectable

Acknowledgements

This work was supported by Basic Science Research Program through the National Research Foundation of Korea (NRF) funded by the Ministry of Education, Science and Technology (2011-0004253).

References

Adams, R.D., Cawley, P., Pye, C.J. and Stone, B.J. (1978), "A vibration technique for nondestructive assessing the integrity of structures", *J. Mech. Eng. Sci.*, **20**(2), 93-100.

Bendat, J.S. and Piersol, A.G. (1993), *Engineering applications of correlation and spectral analysis*, New York, NY, Wiley-Interscience

Bhalla, S. and Soh, C.K. (2003), "Structural impedance based damage diagnosis by piezo-transducers", *Earthq. Eng. Struct. D.*, **32**(12), 1897-1916.

Bhalla, S., Praveen, K., Gupta A. and Datta T.K. (2009), "Simplified impedance model for adhesively bonded piezo-impedance transducers", *J. Aerospace Eng.*, **22**(4), 373-382.

Brincker, R., Zhang. L. and Andersen, P. (2001), "Modal identification of output-only system using frequency domain decomposition", *Smart Mater. Struct.*, **10**(3), 441-445.

Catbas, F.N., Brown, D.L. and Aktan, A.E. (2006), "Use of modal flexibility for damage detection and condition assessment: Case studies and demonstrations on large structures", *J. Struct. Eng.- ASCE*, **132**(11), 1699-1712.

Doebling, S.W., Farrar, C.R. and Prime, M.B. (1998), "A summary review of vibration-based damage identification methods", *Shock Vib.*, **30**(2), 91-105.

Giurgiutiu, V. and Zagrai, A.N. (2005), "Damage detection in thin plates and aerospace structures with the electro-mechanical impedance method", *Struct. Health Monit.*, **4**(2), 99-118.

Gul, M. and Catbas, F.N. (2008), "Ambient vibration data analysis for structural identification and global condition assessment", *J. Eng. Mech.- ASCE*, **134**(8), 650-662.

Kim, J.T., Ryu, Y.S., Cho, H.M. and Stubbs, N. (2003), "Damage identification in beam-type structures: frequency-based method vs mode-shape-based method", *Eng. Struct.*, **25**(1), 57-67.

Kim, J.T., Park, J.H. and Lee, B.J. (2006), "Vibration-based damage monitoring in model plate-girder bridges under uncertain temperature conditions", *Eng. Struct.*, **29**(7), 1354-1365.

Kim, J.T., Na, W.B., Hong, D.S. and Park, J.H. (2006), "Global and local health monitoring of plate-girder bridges under uncertain temperature conditions", *Steel Struct.*, **6**, 369-376

Kim, J.T., Park, J.H., Hong, D.S. and Park, W.S. (2010), "Hybrid health monitoring of prestressed concrete girder bridges by sequential vibration-impedance approaches", *Eng. Struct.*, **32**(1), 115-128

Kim, J.T., Park, J.H., Koo, K.Y. and Lee, J.J. (2008), "Acceleration-based neural networks algorithm for damage detection in structures", *Smart Struct. Syst.*, **4**(5), 583-603.

Koo, K.Y. (2008), *Structural health monitoring methods for bridges using ambient vibration and impedance measurements*, *Doctoral Dissertation*, Korea Advanced Institute of Science and Technology, Deajeon. Korea.

Liang, C., Sun, F.P. and Rogers, C.A. (1996), "Electro-mechanical impedance modeling of active material systems", *Smart Mater. Struct.*, **5**(2), 171-186.

Nagayama, T., Spencer, B.F. and Rice, J.A. (2009), "Autonomous decentralized structural health monitoring using smart sensors", *Struct. Health Monit.*, **16**(7-8), 842-859.

Pandey, A.K., Biswas, M. and Samman, M.M. (1991), "Damage detection from changes in curvature mode s hape", *J. Sound Vib.,***145**(2), 312-332.

Park, G., Cudney, H. and Inman D. (2000), "Impedance-based health monitoring of civil structural components", *J. Infrastruct. Syst.*, **6**(4), 153-160.

Park, G., Sohn, H., Farrar, C. and Inman, D. (2003), "Overview of piezoelectric impedance-based health monitoring and path forward", *Shock Vib.*, **35**(6), 451-463.

Park, J.H., Kim, J.T., Hong, D.S., Mascarenas, D. and Lynch, J.P. (2010), "Autonomous smart sensor nodes for global and local damage detection of prestressed concrete bridges based on accelerations and impedance measurements", *Smart Struct. Syst.*, **6**(5-6), 711-730.

Park, S., Yun, C.B., Roh, Y. and Lee, J.J (2005), "Health monitoring of steel structures using impedance of thickness modes at PZT patches", *Smart Struct. Syst.*, **1**(4), 339-353.

Park, S., Yun, C.B., Roh, Y. And Lee, J.J. (2006), "PZT-based active damage detection techniques for steel bridge components", *Smart Mater. Struct.*, **15**(4), 957-966.

Shanker, R., Bhalla, S., Gupta, A. and Kumar, M.P. (2011), "Dual use of PZT patches as sensors in global dynamic and local electromechanical impedance techniques for structural health monitoring", *J. Intel. Mat. Syst. Str.*, published online on September 2011.

Sim, S.H., Spencer, B.F. and Nagayama T. (2011), "Multimetric sensing for structural damage detection", *J. Eng. Mech.- ASCE*, **137**(1), 22-30

Sirohi, J. and Chopra, I. (2000), "Fundamental understanding of piezoelectric strain sensors", *J. Intel. Mat. Syst. Str.*, **11**(4), 246-257.

Sohn, H. and Farrar, C.R. (2001), "Damage diagnosis using time series analysis of vibration signals", *Smart Mater. Struct.*, **10**(3), 446-451.

Sohn, H., Farrar, C.R., Hemez, F.M., Shunk, D.D., Stinemates, D.W. and Nadler, B.R. (2003), A *review of structural health monitoring literature: 1996-2001*, Los Alamos National Laboratory Report, LA-13976-MS, Los Alamos, NM.

Stubbs, N. and Kim, J.T. (1996), “Damage localization in structures without baseline modal parameters”, *AIAA J.*, **34**(8), 1644-1649.

Sun, F.P., Chaudhry, Z., Rogers, C.A. and Majmundar, M. (1995), “Automated real-time structure health monitoring via signature pattern recognition”, *Proceedings of the SPIE*, San Diego.

Yi, J.H. and Yun, C.B. (2004), “Comparative study on modal identification methods uing output-only information”, *Struct. Eng. Mech.*, **17**(7), 927-944.

Zagrai, A.N. and Giurgiutiu, V. (2001), “Electro-mechanical impedance method for crack detection in thin plates”, *J. Intel. Mat. Syst. Str.*, **12**(10), 709-718.